Unifying model of shoot gravitropism reveals proprioception as a central feature of posture control in plants

Renaud Bastien[a,b,c], Tomas Bohr[d], Bruno Moulia[a,b,1,2], and Stéphane Douady[c,2]

[a]INRA (Institut National de la Recherche Agronomique), UMR0547 (Unité Mixte de Recherche PIAF Physique et Physiologie Intégratives de l'Arbre Fruitier et Forestier), F-63100 Clermont-Ferrand, France; [b]Clermont Université, Université Blaise Pascal, UMR0547 (Unité Mixte de Recherche PIAF Physique et Physiologie Intégratives de l'Arbre Fruitier et Forestier), BP 10448, F-63000 Clermont-Ferrand, France; [c]Matière et Systèmes Complexes, Université Paris-Diderot, 75025 Paris Cedex 13, France; and [d]Department of Physics and Center for Fluid Dynamics, Technical University of Denmark, DK-2800 Lyngby, Denmark

Edited by Przemyslaw Prusinkiewicz, University of Calgary, Calgary, AB, Canada, and accepted by the Editorial Board November 2, 2012 (received for review August 17, 2012)

Gravitropism, the slow reorientation of plant growth in response to gravity, is a key determinant of the form and posture of land plants. Shoot gravitropism is triggered when statocysts sense the local angle of the growing organ relative to the gravitational field. Lateral transport of the hormone auxin to the lower side is then enhanced, resulting in differential gene expression and cell elongation causing the organ to bend. However, little is known about the dynamics, regulation, and diversity of the entire bending and straightening process. Here, we modeled the bending and straightening of a rod-like organ and compared it with the gravitropism kinematics of different organs from 11 angiosperms. We show that gravitropic straightening shares common traits across species, organs, and orders of magnitude. The minimal dynamic model accounting for these traits is not the widely cited gravisensing law but one that also takes into account the sensing of local curvature, what we describe here as a graviproprioceptive law. In our model, the entire dynamics of the bending/straightening response is described by a single dimensionless "bending number" *B* that reflects the ratio between graviceptive and proprioceptive sensitivities. The parameter *B* defines both the final shape of the organ at equilibrium and the timing of curving and straightening. *B* can be estimated from simple experiments, and the model can then explain most of the diversity observed in experiments. Proprioceptive sensing is thus as important as gravisensing in gravitropic control, and the *B* ratio can be measured as phenotype in genetic studies.

perception | signaling | movement | morphogenesis

Plant gravitropism is the growth movement of organs in response to gravity that ensures that most shoots grow up and most roots grow down (1–6). As for all tropisms, a directional stimulus is sensed (gravity in this case), and the curvature of the organ changes over time until a set-angle and a steady-state shape are reached (2, 7, 8). The change in shape is achieved by differential elongation for organs undergoing primary growth (e.g., coleoptiles) or by differential differentiation and shrinkage of reaction wood for organs undergoing secondary growth (e.g., tree trunks) (9). Tropisms are complex responses, as unlike other plant movements (e.g., fast movements) (5, 10) the motor activity generated is under continuous biological control (e.g., refs. 3, 11, 12).

The biomechanics of plant elongation growth has been analyzed in some detail (5, 13, 14), but less is known about the biological control of tropic movements and differential growth (3, 6). Many molecular and genetic processes that occur inside sensing and motor cells have been described (2, 15). For example, statocysts are cells that sense gravity through the complex motion of small intercellular bodies called statoliths (16). However, a huge number of sensing and motor cells act together to produce the growth movements of a multicellular organ. How are the movements of an organ controlled and coordinated biologically? This is a key question, as establishing the correct posture of aerial organs with respect to the rest of the plant has important physiological and ecological consequences (e.g., access to light or long-term mechanical stability) (4).

The gravitropic responses of some plants and even fungi have similar features (8). In essence, this has been described as a biphasic pattern of general curving followed by basipetal straightening (GC/BS) (4, 17). First, the organ curves up gravitropically, then a phase of decurving starts at the tip and propagates downward, so that the curvature finally becomes concentrated at the base of the growth zone and steady (7–9, 18–20). This decurving, which has also been described as autotropic (i.e., the tendency of plants to recover straightness in the absence of any external stimulus) (7, 21), may start before the tip reaches the vertical (4). It is striking that organs differing in size by up to four orders of magnitude (e.g., from an hypocotyl to the trunk of an adult tree) display similar traits, despite great differences in the timing of the tropic movement and the motor processes involved (3). However, there are also differences in the gravitropic responses. Depending on the species and the growth conditions, plants may or may not oscillate transiently about the stimulus axis or reach a proper alignment with the direction of the stimulus (e.g., ref. 8).

Currently, the phenotypic variability of the GC/BS biphasic pattern over a broad sample of species is, however, hard to estimate quantitatively, as most studies of gravitropism have only focused on measuring the tip angle (3). As we shall demonstrate, it is necessary to specify the local curvature C (or equivalently, the inclination angle A) over the entire growth zone (Fig. 1) and how it changes over time. If this is done, it is possible to build up a minimal dynamic model for tropic movements in space. This can be combined with dimensional analysis (as is used in fluid mechanics, for example) to characterize the size and time dependencies and set up dimensionless control parameters. This then makes it possible to compare experiments with predictions from the model quantitatively over a broad taxonomical sample of species with very different sizes and growth velocities and to reveal universal behaviors and controlling mechanisms.

The gravitropic responses of 12 genotypes from 11 plant species were studied, representing a broad taxonomical range of land angiosperms (*SI Appendix*, Fig. S4), major growth habits (herbs, shrubs, and trees), as well as different uses (agriculture, horticulture, and forestry but also major laboratory model plants for genetics and physiology). Different types of organs were studied: coleoptile, hypocotyl, epicotyl, herbaceous and woody

Author contributions: B.M. and S.D. designed research and hypotheses; R.B. developed the models, the experiments, and the numerical simulations; R.B. and T.B. solved the equations; R.B., B.M., and S.D. analyzed data; and R.B., T.B., B.M., and S.D. wrote the paper.

The authors declare no conflict of interest.

This article is a PNAS Direct Submission. P.P. is a guest editor invited by the Editorial Board.

[1]To whom correspondence should be addressed. E-mail: bruno.moulia@clermont.inra.fr.

[2]B.M. and S.D. contributed equally to this work.

This article contains supporting information online at www.pnas.org/lookup/suppl/doi:10.1073/pnas.1214301109/-/DCSupplemental.

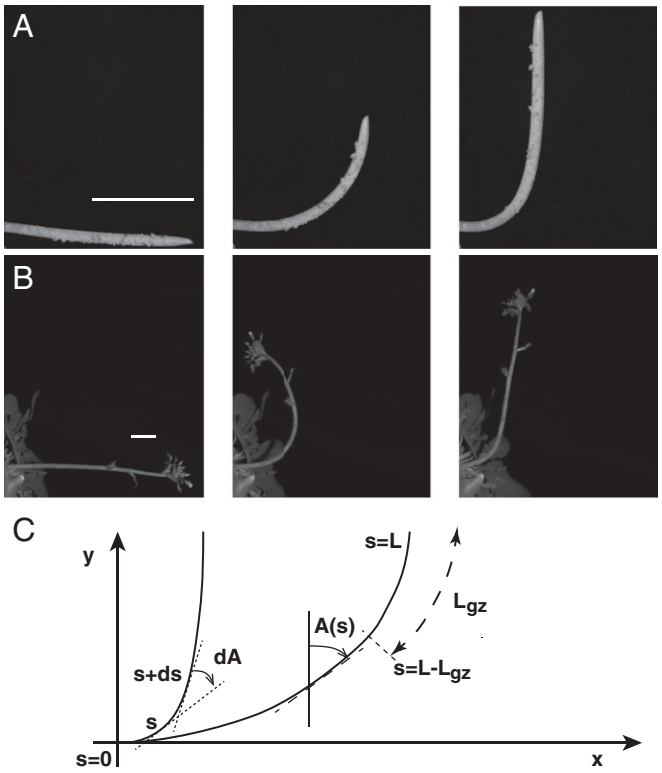

Fig. 1. Successive shapes formed by plant organs undergoing gravitropism and a geometrical description of these shapes. (*A*) Time-lapse photographs of the gravitropic response of a wheat coleoptile placed horizontally (Movie S1). (*B*) Time-lapse photographs of the gravitropic response of an *Arabidopsis* inflorescence placed horizontally (Movie S2). White bars, 1 cm. (*C*) Geometric description of organ shape. The median line of an organ of total length L is in a plane defined by coordinates x, y. The arc length s is defined along the median line, with $s = 0$ referring to the base and $s = L$ referring to the apex. In an elongating organ, only the part inside the growth zone of length L_{gz} from the apex is able to curve (with $L_{gz} = L$ at early stages and $L_{gz} < L$ later on), whereas the whole length is able to curve in organs undergoing secondary growth (i.e., $L_{gz} = L$). $A(s)$ is the local orientation of the organ with respect to the vertical and $C(s)$ the local curvature. The two curves shown have the same apical angle $A(L)$ but different shapes, so to specify the shape we need the form of $A(s)$ or $C(s)$ along the entire median. Due to the symmetry of the system around the vertical axis, the angle A is a zenith angle—that is, it is zero when the organ is vertical and upright. Thus, an orthotropic organ has a gravitropic set point angle of 0. For simplicity, clockwise angles are considered as positive.

vegetative stems, and inflorescence stems, representing the two types of tropic motors (differential elongation growth, reaction woods) and varying by two orders of magnitude in organ size and in the timing of the tropic movements. Organs were tilted horizontally and the gravitropic growth was recorded through time-lapse photography.

All of the plant organs studied first curved upwards before eventually reaching a near vertical steady-state form where the apical part was straight, as shown for two examples in Fig. 1 and in Movies S1 and S2. The images were used to generate color maps of the curvature of the organ in space (along the organ) and time, as shown for three examples in Fig. 2. Shortly after plants were placed horizontally, the dominant movement observed was a rapid up-curving (negatively gravitropic) along the entire organ. However, the apex soon started to straighten and the straightening gradually moved downward along the organ. Finally, the curvature tended to concentrate at the base of the growth zone, becoming fixed there. Such a typical GC/BS behavior was observed in all 12 cases studied, despite differences of around two orders of magnitude in organ sizes and convergence time, the time T_c taken for the organ to return to a steady state, ranging from several hours to several months.

Despite the common properties of the response, time lapse photography showed that plant organs acted differently when approaching the vertical. The apices of some plant organs never overshot the vertical (Fig. 1*A*), whereas others did so several times, exhibiting transient oscillations with the formation of C- or even S-shapes (Fig. 1*B*). Thus, a minimal dynamic model of gravitropism has to explain both the common biphasic GC/BS pattern and the diversity in transient oscillation and convergence time.

According to the literature, the current qualitative model of gravitropism in aerial shoots is based on the following hypotheses:

H1: Gravisensing is exclusively local; each element along the length of the organ is able to respond to its current state (22), since statocysts are found all along the growth zone (16). Gravisensing by the apex does not have a special influence (e.g., the final shapes of organs after decapitation are similar to intact controls) (1, 23).

H2: The local inclination angle A (Fig. 1) is sensed. This sensing follows a sine law (3, 6) (see below).

H3: In our reference frame, the so-called gravitropic set angle (GSA) (24) is equal to 0 (Fig. 1) so the motion tends to bring the organ upward toward the vertical (this corresponds to the botanical term "negative ortho-gravitropism," a most common feature in shoots).

H4: The action of the tropic motor is fully driven by the perception–regulation process and results in a change in the local curvature through differential growth and/or tissue differentiation. This response can only be expressed where differential growth and differentiation occurs, namely in the "growth zone" of length L_{gz} (3).

To form a mathematical model, we shall describe the shape of the organ in terms of its median—that is, its central axis (Fig. 1). We parameterize the median by the arc length s going from the base $s = 0$ to the apex $s = L$, and the angle $A(s,t)$ describes the local orientation of the median with respect to the vertical at time t. The corresponding local curvature $C(s,t)$ is the spatial rate of change of A along s and from differential geometry we know that:

$$C(s,t) = \partial A(s,t)/\partial s \text{ or } A(s,t) = A_0 + \int_0^s C(l,t)dl. \qquad [1]$$

The so-called "sine law" was first defined by Sachs in the 19th century and has been widely used since (see ref. 3 for a review). It can be expressed as a relationship between the change in the local curvature and the local angle as in:

$$\partial C(s,t)/\partial t = -\beta \sin A(s,t), \qquad [2]$$

where β is the apparent gravisensitivity. Note that Eq. **2** is unchanged when A changes to $-A$ and C changes to $-C$, as would be expected. This model is only valid in the growth zone, $s > (L - L_{gz})$, where L is the total organ length and L_{gz} is the length of the effective zone where active curving can be achieved. Outside this region, the curvature does not change with time.

In this model, changes in the overall length of the organ are not taken into account. This is quite reasonable in the case of woody organs, as they undergo curving through relatively small maturation strains in reaction woods, but it is less applicable to organs curving through differential elongation (3, 14). In expanding organs, each segment of the organ in the growth zone "flows" along the organ being pushed by the expansion growth of distal elements (3, 14) so Eq. **2** would remain valid only in

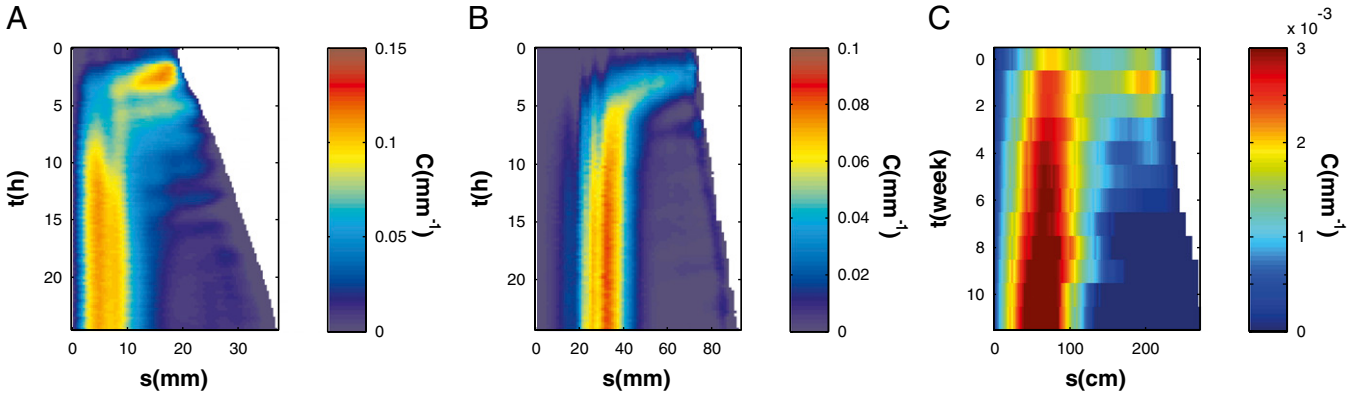

Fig. 2. Kinematics of the entire tropic movement of tilted plant organs shown as color maps plotting the curvature $C(s,t)$ with respect to time t and curvilinear abscissa s (the arc length along the median measured from the base to apex of the organ; Fig. 1). (*A*) Wheat coleoptile (*Triticum aestivum* cv. Recital). The yellow bar is 1 cm long. (*B*) *Arabidopsis* inflorescence (*A. thaliana* ecotype Col0). The yellow bar is 1 cm long. (*C*) Poplar trunk (Hybrid *Populus deltoides x nigra* cv I4551), reprocessed data from ref. 9.

a "comoving" context. To fully specify the changes in curvature, we would thus have to introduce local growth velocities into the model, replacing the derivative in Eq. **2** with the comoving derivative $DC(s,t)/Dt = \partial C(s,t)/\partial t + v(s,t)\partial C(s,t)/\partial s$, where $v(s,t)$ is the local growth velocity. However, in tropic movement, the growth velocities are generally small compared with tropic bending velocities (and the length of the organ that has left the growth zone during the straightening movement is also small) (14), so $DC(s,t)/Dt \approx \partial C(s,t)/\partial t$. The limits of this approximation will be discussed.

To obtain a more tractable model, which we shall solve analytically, we can use the approximation $\sin A \approx A + O(A^3)$ and approximate Eq. **2** by:

$$\partial C(s,t)/\partial t = -\beta A(s,t), \qquad [3]$$

where we note that the $A \to -A$ symmetry is retained. Because in our experiments $|A|$ did not exceed $\pi/2$ and because we are primarily interested in values near zero, this is a reasonable approximation (3). It should be noted that $A(s,t)$ and $C(s,t)$ are not independent, as any further variation in curvature modifies the apical orientation through the "lever-arm effect" expressed in Eq. **1**. In other words, the effect of changes in curvature on downstream orientation angles is amplified by the distance along the organ (3).

The solution of Eq. **3**, which we shall call the "A model," is:

$$A = A_0 J_0\left(2\sqrt{\beta t s}\right); \quad C = A_0\sqrt{\frac{\beta t}{s}} J_1\left(2\sqrt{\beta t s}\right), \qquad [4]$$

where J_n are Bessel functions of the first kind of order n. It has interesting properties. Firstly, the angle A does not depend on space s and time t individually, but only on the combination of $\sqrt{ts}$ and $\sqrt{t/s}$ and is thus an oscillatory function of $\sqrt{ts}$. However, the dynamics of the A model demonstrates that such a system cannot reach a vertical steady state when tilted and clamped at its base (Fig. 3*A* and Movie S3). Indeed, the only steady state in Eq. **3** is $A(s,t) = 0$, but this is forbidden by the basal clamping of the organ fixing $A(s=0,t) = \pi/2$ for all t. Oscillations therefore go on indefinitely, whereas their wavelengths decrease with time. Numerical simulations of Eqs. **3** or **2** displayed the same behavior (*SI Appendix* Fig. S2). This does not agree with any of the experimental results. The A model based on the sine law is therefore not a suitable dynamic model of the gravitropic straightening movement and has to be rejected. To account for the steady state attained after tilting, another hypothesis needs to be introduced:

H5: Each constituent element of the organ perceives its local deformation, the curvature, and responds in order to restore local straightness (7, 19). In animal physiology, this type of sensing is generally called "proprioception," a self-sensing of posture or orientation of body parts relative to the rest of the organism (25). This is not an unreasonable assumption as it is known experimentally that (*i*) plants can sense imposed bending (26, 27) and (*ii*) the curvature of the organ and subsequent mechanical loads have a direct effect on

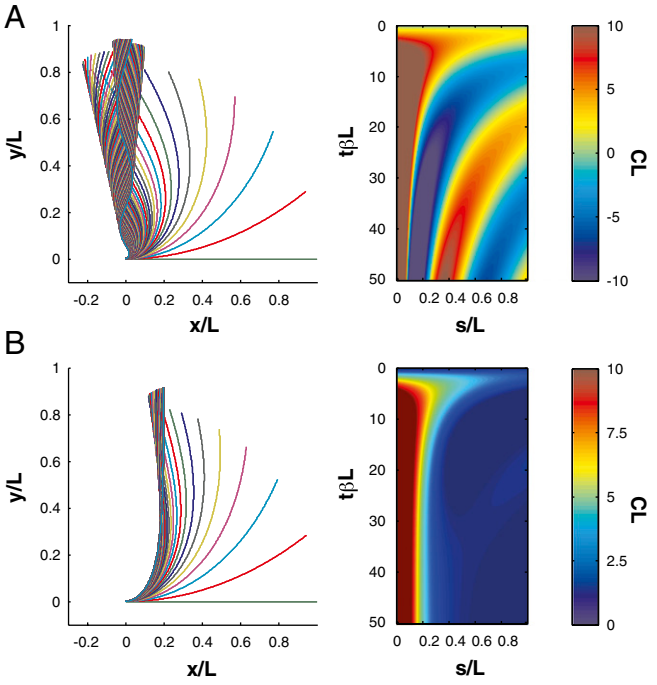

Fig. 3. Solutions of the dimensionless A and AC models. (*Left*) Time-lapse shapes along the movement. (*Right*) Color-coded space–time maps of curvature $C_{th}(s,t)$. (*A*) Graviceptive A model where the response only depends on the local angle. As the organ approaches the vertical, the basal part continues to curve. The organ overshoots the vertical, and the number of oscillations increases with time (Movie S3). (*B*) Graviproprioceptive AC model where the response also depends on the local angle and the local curvature. Here the curvature decreases before reaching the vertical. It does exhibit an S shape, but oscillations are dampened, and the organ converges to a solution where the curvature is focused near the base (Movies S4 and S5).

the orientation of microtubules that may then modify the rate of differential growth (28, 29).

This hypothesis yields a model called the "graviproprioceptive" model, or the "*AC* model":

$$\partial C(s,t)/\partial t = -\beta A(s,t) - \gamma C(s,t), \quad [5]$$

in the growth zone (i.e., for $s > L - L_{gz}$), and 0 elsewhere. Here the change in curvature is directly related to the local curvature itself via the parameter γ, the proprioceptive sensitivity. A more systematic derivation of the *A* and *AC* models from symmetry arguments and rod kinematics is given in *SI Appendix*. The solution of the *AC* model has the form:

$$\begin{aligned} A(s,t) &= A_0 e^{-\gamma t} \sum_{n=0}^{\infty} \left(\frac{\beta s}{\gamma^2 t}\right)^{-n/2} J_n\left(2\sqrt{\beta t s}\right) \\ &= A_0 e^{-\beta s/\gamma} - A_0 \sum_{n=1}^{\infty} (-1)^n \left(\frac{\beta s}{\gamma^2 t}\right)^{n/2} J_n(2\sqrt{\beta t s}), \end{aligned} \quad [6]$$

where it is seen that the dependence on $\sqrt{ts}$ and $\sqrt{t/s}$ is retained, but there is now an infinite sequence of Bessel functions. The first of the two expressions is appropriate for short times. The latter is appropriate for long times and shows that the oscillations are now dampened toward a final steady state, whose form is:

$$A_f(s) = A_0 e^{-\beta s/\gamma} = A_0 e^{-s/L_c}. \quad [7]$$

The dynamics of the *AC* model (Fig. 3*B* and Movies S4 and S5) is now qualitatively consistent with the experiments: the oscillations are dampened, and the organ converges to a steady state where the curvature is focused near the base through a typical GC/BS biphasic pattern.

The convergence length $L_c = \gamma/\beta$ is given by the decay length of the exponential toward the vertical, and it results from the balance between graviception and proprioception. The *AC* model thus gives a direct explanation of the common BS (autotropic) phase, where curvature starts to decrease before reaching the vertical (7, 20). For purely geometrical reasons (lever-arm effect, Eq. **1**), the apical angles decrease faster than the basal angles. Thus, curvature sensing first takes over gravisensing at the tip and decurving starts there. It then moves downward together with the decrease of *A* without any need for a systemic basipetal propagative signal. Another important scale is L_{gz}, the effective length of the growth zone where active curving can be achieved. The ratio $B_l = L_{gz}/L_c = \beta L_{gz}/\gamma$ is a dimensionless number that controls important aspects of the dynamics.

To assess whether the organ has time to converge to a steady state before the apex crosses the vertical, thereby avoiding overshooting, the time of convergence T_c can be compared with the time required for the apex to first reach the vertical, T_v. Using Eq. **5**, T_c can be approximated from the proprioceptive term that dominates when approaching convergence as $T_c = 1/\gamma$ and T_v can be approximated as $T_v = 1/(\beta L_{gz})$ from the graviceptive term dominating initial dynamics. This gives a "temporal" dimensionless number $B_t = T_c/T_v = \beta L_{gz}/\gamma$, which is actually identical to B_l. The fact that $B_t = B_l$ gives a direct link between convergence timing, transient modes, and steady-state form (i.e., a kind of form-movement equivalence). We call this number the "bending number" denoted by *B*.

To compare theory and experiments, *B*, L_{gz}, and L_c were measured morphometrically from initial and steady-state images as shown for *Arabidopsis* inflorescence in Fig. 4. Because L_{gz} is the length of the organ that has curved during the experiment, it can be directly estimated by comparing the two images. By definition, L_c can be measured directly on the image of the final shape as the characteristic length of the curved part (Fig. 4). The bending number *B* ranged from around 0.9–9.3 displaying broad intraspecific and interspecific variability over the experiments. Therefore, the *AC* model can be assessed from them.

The kinematic data from wheat, *Arabidopsis*, and poplar was analyzed in more detail to track the tropic movement after tilting (Fig. 1). The analytical solution $A_{ac}(s,t)$ for the *AC* model (Eq. **6**) was compared with the experimental angle space-time maps, given the bending number value. Angles were chosen instead of curvature here, as otherwise the determination of curvature would involve a derivative, producing more noise. The initial value of *B* for parameter estimation was estimated morphometrically. As the *AC* model does not account for elongation growth, we trimmed the data for wheat and *Arabidopsis* to the length of the growth zone at the beginning of the experiment, as shown in Fig. 5. Typical results from *Arabidopsis* inflorescences are shown in Fig. 5, and additional results from *Arabidopsis*, wheat, and poplar are provided in *SI Appendix*, Figs. S6, S7, and S8, respectively. The *AC* model was found to capture the common features of the angle space-time maps over the entire GC/BS process (compare Fig. 5 *A* and *B*). The (dimensionless) mean slope of comparison of the model vs. data (for the three species together) was 1.00 ± 0.15, the intercept was 0.07 ± 0.20, and the coefficient of determination was 0.92 ± 0.05, so the *AC* model captured around 90% of the total experimental variance in $A(s,t)$ and displayed no mean quantitative bias.

The form–movement equivalence predicted by the *AC* model was then directly assessed through a simple morphometric analysis of the tilting experiments on the 12 angiosperm genotypes. More precisely, we assessed whether the *AC* model predicted the discrete transitions between transient oscillatory modes around the vertical (e.g., Fig. 1 and *SI Appendix*, Fig. S5) with increasing values of the bending number *B*. At a given time *t*, the current mode is defined as the number of places below the apex where the tangent to the central line of the organ is vertical (*SI Appendix*, Fig. S5). If there is one vertical tangent more basal than the apex, then the organ overshoots the vertical once. This is mode 1, when a C shape is formed. If an S shape develops, then the transient mode will be mode 2, and a Σ shape is mode 3, and so on. The mode number *M* of the whole movement is then given by the maximal mode of all of the transitory shapes (e.g., in *SI Appendix*, Fig. S5, the mode of the movement of the inflorescence is $M = 1$ as a transient C shape is seen but not an S shape). In Fig. 6, the modes of 12 plant organ responses were plotted against the respective estimated bending numbers and compared with the predictions of the *AC* model.

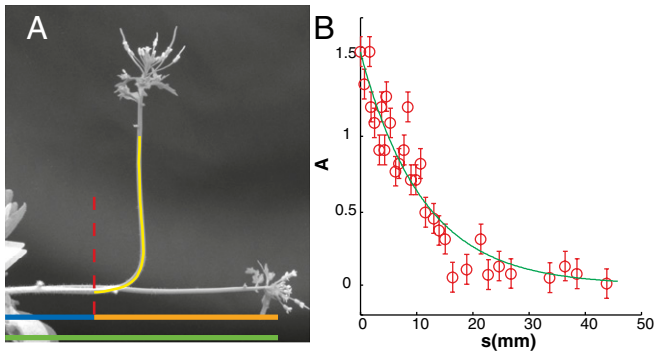

Fig. 4. Morphometric measurement of the bending number *B* from steady-state configurations of *Arabidopsis* inflorescences. (*A*) Estimation of the effective length L_{gz} by superimposing the first and last kinematics images. The red dotted lines indicate the zone where the organ started to curve. The effective length of the organ can then be defined as the distance from this point to the apex of the initial plant on the first image. (*B*) Estimation of the convergence length L_c by plotting the local inclination angle $A(s,t)$ along the organ beginning from the curved zone. To extract the convergence length L_c, the angle $A(s,t)$ is fitted with the exponential $A(s,t) = A_0 e^{-s/L_c}$, $n = 28$, $R^2 = 0.99$.

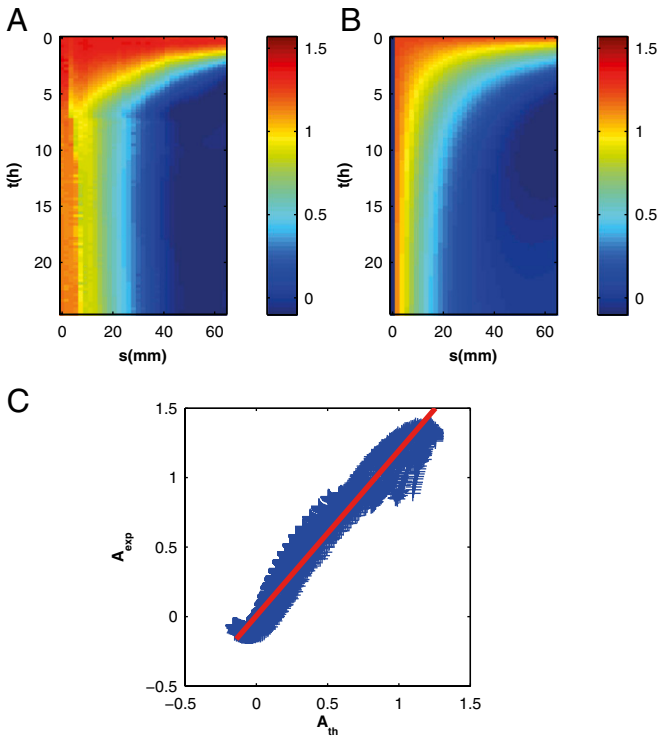

Fig. 5. Quantitative comparison between experimental (exp) and predicted (th) angle space–time maps of $A(s,t)$ for an *Arabidopsis* inflorescence for the whole gravitropic response. (*A*) Experimental angle space–time map of $A_{exp}(S,t)$ trimmed for $s \leq L(t=0)$, as the *AC* model does not consider changes in length. (*B*) Angle space–time map predicted by the *AC* model $A_{ac}(s,t)$. (*C*) Quantitative validation plot of experimental $A_{exp}(s,t)$ vs. theoretical $A_{th}(s,t)$. Orthogonal linear fit slope, 1.13; intercept, 0.17; $R^2 = 0.94$.

The prediction displays stepwise increases in modes at bending numbers corresponding to 2.8 for the transition from mode 0 to mode 1 and 3.9 for the transition from mode 1 to mode 2. No plant in the experiments displayed mode transitions for smaller bending numbers than was predicted by the *AC* model. Many individual plant responses were found near the transition from mode 0 to mode 1—that is, between the mode in which they cannot reach the vertical and the mode where they overshoot the vertical and oscillate. The transition from mode 2 to mode 3 only occurs for very large bending numbers ($B > 10$) and was never seen in any of the experiments. In two-thirds of the plants, the prediction of the oscillations by the *AC* model was correct. However, about one-third of the plants oscillated less than predicted. To some extent, this may be due to inaccuracies in the estimation of bending numbers, but second-order mechanisms (possibly related to elongation growth) are likely to be involved, ones that add to the common gravipriproprioceptive core described by the *AC* model.

Nevertheless, the fact that the *AC* model accounts for the common GC/BS pattern with no quantitative bias and captures the transitions between three different modes over one order of magnitude of bending numbers and a broad taxonomical range is an indication of its robustness. All this strongly suggests that hypothesis 5 and its mathematical description by the *AC* model captures the universal core of the control over gravitropic dynamics. The longstanding sine law for gravitropism (3) should thus be replaced by the gravipriproprioceptive dynamic *AC* model, which highlights the equal importance of curvature- and gravisensing. Doing so has already yielded three major insights.

i) The *AC* model can achieve distinct steady-state tip angles for the same vertical GSA. In particular, plants with $B < 2.8$ cannot reach their GSA (as specified in the gravitropic term of the *AC* model) even in the absence of biomechanical and physiological limits in their motor bending capacity (3, 10, 12). Therefore, the GSA cannot be measured directly from experiments and can only be assessed by *AC* model–assisted phenotyping.

ii) The fact that most plants display very few oscillations before converging to the steady state despite destabilization through lever-arm effects does not actually require the propagation of long-distance biological signals and complex regulation. The value of the dimensionless bending number simply has to be selected in the proper range—that is, graviceptive and proprioceptive sensitivities have to be tuned together as a function of organ size possibly pointing to molecular mechanisms yet to be discovered.

iii) The *AC* model can account for the behavior of actively elongating organs despite neglecting the effects of mean elongation growth. Subapical elongation growth may have destabilizing effects by spreading curvature, convecting, and fixing it outside the growth zone in mature tissues (14). Our result means that the values for the time of convergence to the steady-state T_c were small enough compared with the characteristic times for elongation growth in all of the species studied. As T_c depends mostly on the proprioceptive sensitivity, possibly there is natural selection for this trait as a function of the relative elongation rate (and organ slenderness) and for fine physiological tuning.

Proprioceptive sensing is thus as important as gravisensing for gravitropism. The study of molecular sensing mechanisms (2, 15) can thus now be extended to the cross-talk between gravi- and propriosensing as a function of organ size. Candidate mechanisms for the proprioception of the curvature may involve mechanical strain- or stress-sensing (27, 30) triggering microtubules reorientation (28, 29). Ethylene seems to be involved (17) but not the lateral transport of auxin (21). Whatever the detailed mechanisms involved, putative models of molecular networks controlling gravipriproprioceptive sensing (31) should be consistent with the *AC* model and with the existence of a dimensionless control parameter, the bending number. Moreover, the bending number B is a real quantitative genetic trait (32, 33). It controls the whole dynamics of tropic movement and encapsulates both the geometry

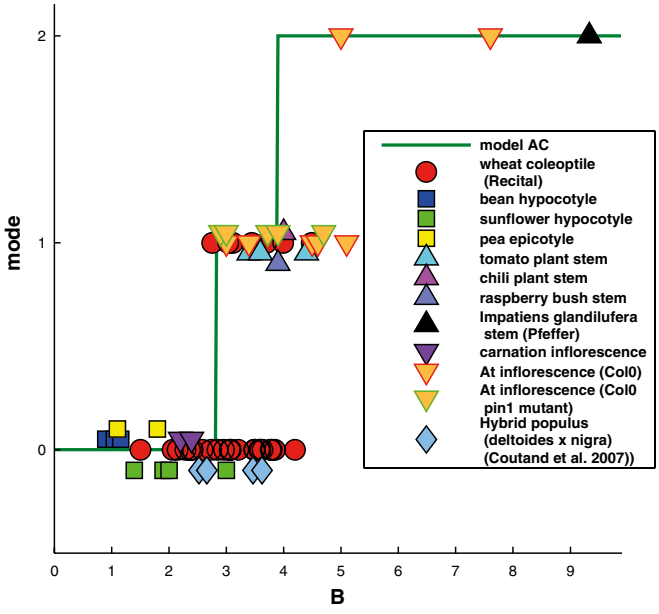

Fig. 6. Mode number M plotted against bending number $B = L_{gz}/L_c$ for individual plants ($N = 67$). The green line shows the same plot for the *AC* model.

and the perception–regulation functions involved (34). The simple measurement of B is now possible and this may be used for the high-throughput phenotyping of mutants or variants in many species. From a more general perspective, it would now be interesting to explore how plants manage to control gravitropism despite the destabilizing effects of elongation growth. Areas to investigate are whether there is physiological tuning of B during growth and whether there is natural selection for proprioceptive sensitivity as a function of the relative elongation rate and organ slenderness. For this, it will be necessary to combine noninvasive kinematics methods to monitor elongation growth at the same time as curvature (e.g., refs. 32, 33) with a more general model that explicitly includes the expansion and convection of cells during growth (3, 14). Finally, this approach can also be used to study the gravitropism of other plant organs and other growth movements like phototropism or nutation, which will show whether this theory of active movement is universal.

Materials and Methods

Experiments were conducted in growth cabinets for etiolated wheat coleoptiles (*Triticum aestivum* cv. Recital) or controlled temperature greenhouses for the nine other types of plant organs—bean hypocotyl (*Phaseolus vulgaris*), sunflower hypocotyl (*Helianthus annuus*), pea epicotyl (*Pisum sativum*), tomato stem (*Solanum lycopersicum*), chili stem (*Capsicum annuum*), raspberry cane (*Rubus ideaus*), carnation inflorescence (*Dianthus caryophyllus*), and *Arabidopsis thaliana* inflorescences from a wild-type (ecotype Col0) and its *pin1* mutant [a mutant of the PIN1 auxin efflux carier displaying reduced auxin longitudinal transport (11) (see *SI Appendix*, sections S2.1 and S2.4 for more details)]. Plants were grown until a given developmental stage of the organ of interest (e.g., until the beginning of inflorescence flowering for *Arabidopsis* in Fig. 4). They were then tilted and clamped horizontally $A(s = 0, t) = \phi/2$ for all t under constant environmental conditions in the dark (to avoid interactions with phototropism). Number of replicates were 30 for wheat, 15 for *Arabidopsis*, and 5 for all the other species. Published data were also reprocessed from similar experiments on *Impatiens glandilufera* stems by Pfeffer (35) and on poplar trunks (*Populus deltoides x nigra* cv I4551) by Coutand et al. (9). More precisely, two types of experiments were conducted, as explained in *SI Appendix*, section S2.2 and S2.5: (*i*) detailed kinematics experiments on two model species (*Arabidopsis* and wheat), based on time-lapse photography and quantitative analysis of curving-decurving kinematics (*SI Appendix*, sections S2.2 to S2.4) and (*ii*) simplified morphometric experiments on all the genotypes, to estimate the bending number (through $B_l = L_{gz}/L_c$) and the (transient) global mode M, defined as the maximum number of places below the apex where the tangent to the central line of the organ is vertical (*SI Appendix*, Fig. S5 and section S2.5). Quantitative assessment of the *AC* model was conducted by fitting Eq. **6** to the datasets from the detailed kinematics experiments (including also poplar; see *SI Appendix*, section S2.6), whereas a qualitative assessment on mode transitions and space-time equivalence was conducted on the dataset from the morphometric experiment (including also *Impatiens*; see *SI Appendix*, section S2.5).

ACKNOWLEDGMENTS. We thank Dr. C. Coutand for providing the poplar data, S. Ploquin and Dr. C. Girousse for help with the wheat experiments, Drs. A. Peaucelle and H. Hofte for help with the *Arabidopsis* experiments, and Emondo (Boston) for editing the English.

1. Darwin C (1880) *The Power of Movements in Plants* (D. Appleton and Company, New York).
2. Gilroy S, Masson PH (2008) *Plant Tropisms* (Blackwell, Oxford).
3. Moulia B, Fournier M (2009) The power and control of gravitropic movements in plants: A biomechanical and systems biology view. *J Exp Bot* 60(2):461–486.
4. Moulia B, Coutand C, Lenne C (2006) Posture control and skeletal mechanical acclimation in terrestrial plants: Implications for mechanical modeling of plant architecture. *Am J Bot* 93(10):1477–1489.
5. Skotheim JM, Mahadevan L (2005) Physical limits and design principles for plant and fungal movements. *Science* 308(5726):1308–1310.
6. Galland P (2002) Tropisms of Avena coleoptiles: Sine law for gravitropism, exponential law for photogravitropic equilibrium. *Planta* 215(5):779–784.
7. Firn RD, Digby J (1979) A study of the autotropic straightening reaction of a shoot previously curved during geotropism. *Plant Cell Environ* 2(2):149–154.
8. Stockus A, Moore D (1996) Comparison of plant and fungal gravitropic responses using imitational modelling. *Plant Cell Environ* 19(7):787–800.
9. Coutand C, Fournier M, Moulia B (2007) The gravitropic response of poplar trunks: Key roles of prestressed wood regulation and the relative kinetics of cambial growth versus wood maturation. *Plant Physiol* 144(2):1166–1180.
10. Forterre Y, Skotheim JM, Dumais J, Mahadevan L (2005) How the Venus flytrap snaps. *Nature* 433(7024):421–425.
11. Noh B, Bandyopadhyay A, Peer WA, Spalding EP, Murphy AS (2003) Enhanced gravi- and phototropism in plant mdr mutants mislocalizing the auxin efflux protein PIN1. *Nature* 423(6943):999–1002.
12. Bennett MJ, Roberts I, Palme I (2000) Moving on up: Auxin-induced K+ channel expression regulates gravitropism. *Trends Plant Sci* 5(3):85–86.
13. Goriely A, et al. (2008) Elastic growth models. *Mathematical Modelling of Biosystems*, ed Mondaini R (Springer-Verlag, Berlin and Heidelberg), pp 1–44.
14. Silk WK (1984) Quantitative descriptions of development. *Annu Rev Plant Physiol* 35: 479–518.
15. Blancaflor EB, Masson PH (2003) Plant gravitropism. Unraveling the ups and downs of a complex process. *Plant Physiol* 133(4):1677–1690.
16. Morita MT (2010) Directional gravity sensing in gravitropism. *Annu Rev Plant Biol* 61(1):705–720.
17. Pickard BG (1985) Roles of hormones, protons and calcium in geotropism. *Encyclopedia of Plant Physiology*, eds Phais RP, Reid DM (Springer, Berlin), Vol III, pp 193–281.
18. Stankovic B, Volkmann D, Sack FD (1998) Autotropism, automorphogenesis, and gravity. *Physiol Plant* 102(2):328–335.
19. Meskauskas A, Moore D, Novak Frazer L (1998) Mathematical modelling of morphogenesis in fungi: Spatial organization of the gravitropic response in the mushroom stem of *Coprinus cinereus*. *New Phytol* 140(1):111–123.
20. Meskauskas A, Novak Frazer L, Moore D (1999) Mathematical modelling of morphogenesis in fungi: A key role for curvature compensation ("autotropism") in the local curvature distribution model. *New Phytol* 143(2):387–399.
21. Haga K, Iino M (2006) Asymmetric distribution of auxin correlates with gravitropism and phototropism but not with autostraightening (autotropism) in pea epicotyls. *J Exp Bot* 57(4):837–847.
22. Kuznetsov OA, Hasenstein KH (1997) Magnetophoretic induction of curvature in coleoptiles and hypocotyls. *J Exp Bot* 48(316):1951–1957.
23. Firn RD, Digby J, Hall A (1981) The role of the shoot apex in geotropism. *Plant Cell Environ* 4(2):125–129.
24. Digby J, Firn RD (1995) The gravitropic set-point angle (GSA): The identification of an important developmentally controlled variable governing plant architecture. *Plant Cell Environ* 18(12):1434–1440.
25. Sherrington CS (1907) On the proprio-ceptive system, especially in its reflex aspect. *Brain* 29(4):467–482.
26. Coutand C, Moulia B (2000) Biomechanical study of the effect of a controlled bending on tomato stem elongation: Local strain sensing and spatial integration of the signal. *J Exp Bot* 51(352):1825–1842.
27. Moulia B, et al. (2011) Integrative mechanobiology of growth and architectural development in changing mechanical environments. *Mechanical Integration of Plant Cells and Plants*, ed Wojtaszek Springer P (Springer, Berlin), pp 269–303.
28. Fischer K, Schopfer P (1998) Physical strain-mediated microtubule reorientation in the epidermis of gravitropically or phototropically stimulated maize coleoptiles. *Plant J* 15(1):119–123.
29. Ikushima T, Shimmen T (2005) Mechano-sensitive orientation of cortical microtubules during gravitropism in azuki bean epicotyls. *J Plant Res* 118(1):19–26.
30. Hamant O, et al. (2008) Developmental patterning by mechanical signals in Arabidopsis. *Science* 322(5908):1650–1655.
31. Rodrigo G, Jaramillo A, Blázquez MA (2011) Integral control of plant gravitropism through the interplay of hormone signaling and gene regulation. *Biophys J* 101(4): 757–763.
32. Miller ND, Parks BM, Spalding EP (2007) Computer-vision analysis of seedling responses to light and gravity. *Plant J* 52(2):374–381.
33. Brooks TL, Miller ND, Spalding EP (2010) Plasticity of Arabidopsis root gravitropism throughout a multidimensional condition space quantified by automated image analysis. *Plant Physiol* 152(1):206–216.
34. Coen E, Rolland-Lagan AG, Matthews M, Bangham JA, Prusinkiewicz P (2004) The genetics of geometry. *Proc Natl Acad Sci USA* 101(14):4728–4735.
35. Pfeffer WTG (1898–1900) Kinematographische Studien an Impatiens, Vicia, Tulipa, Mimosa und Desmodium [Kinematics Studies of an Impatiens, Vicia, Tulipa, Mimosa and Desmodium] (Timelapse Photography, Color: No, Sound: No, 3min 30) (Universität Leipzig, Botanisches Institut, Leipzig, Germany). Video transcription by Kinescope. Available at www.dailymotion.com/video/x1hp9q/. Accessed November 20, 2012.

A unifying model of shoot gravitropism reveals proprioception as a central feature of posture control in plants - supplementary information-

Renaud Bastien [*] [†] [‡], **Tomas Bohr** [§], **Bruno Moulia** [*] [†] [¶] **and Stéphane Douady** [‡] [¶]

[*]INRA, UMR547 PIAF Physique et physiologie Intégratives de l'Arbre fruitier et Forestier, F-63100 Clermont-Ferrand, France ,[†]Clermont Université, Université Blaise Pascal, UMR547 PIAF Physique et physiologie Intégratives de l'Arbre fruitier et Forestier , BP 10448, F-63000 Clermont-Ferrand, France,[‡]Matière et Systèmes Complexes, Université Paris-Diderot, 10 rue Alice Domont et Léonie Duquet, 75025 Paris Cedex 13, France,[§]Department of Physics and Center for Fluid Dynamics, Technical University of Denmark, DK-2800 Lyngby, Denmark, and [¶]These authors have contributed equally and complementary to the work

1- Construction of the mathematical model

1.1 General equation. The plant organs considered in this study are slender structures. During tropic movements cells do not undergo shear growth and torsion can be neglected (3). Therefore the organ can be considered mechanically as an (actively) flexing rod (3). Its successive shapes can thus be fully described by the local orientation $A(s,t)$ and the local curvature $C(s,t)$ fields. Note that curvature C is an objective quantity defining the local shape of the organ irrespective of its local inclination A. The mechanism that produces the movement, like differential growth, modifies the local curvature of the organ. The equation that drives the system should thus determine the temporal variation in the local curvature

$$\frac{\partial C(s,t)}{\partial t} = \phi, \qquad [1]$$

where ϕ is a function of the geometry, the biomechanics of bending and the perception-regulation process, s is the curvilinear abscissa from the base to the apex and t is the time elapsed since the plant was tilted horizontally. It is postulated that the perception-regulation process driving the dynamics of the movement is of the first order, i.e. that the biomechanical motors are not limiting the movement as is often the case (3). In addition, the perception involved in gravitropism is local (see the argument for Hypothesis H1 in the main text). The perception of a segment at position s should be a function of the local angle and curvature $A(s,t)$ and $C(s,t)$, and this local perception then results in a local response. Equation [1] can thus be rewritten

$$\frac{\partial C(s,t)}{\partial t} = \phi(A, C). \qquad [2]$$

Assuming that both the tilting angle $A(s,t)$ and the curvature $C(s,t)$ are small, the function ϕ can be expanded as polynomials of $A(s,t)$ and $C(s,t)$ near the vertical (straight) configurations of the organ.

$$\begin{aligned}\frac{\partial C(s,t)}{\partial t} &= \alpha + \beta_1 A + \beta_2 A^2 + ... + \gamma_1 C + \gamma_2 C^2 + ... + \\ &\quad + \delta_1 AC + \delta_2 A^2 C + \delta_3 A C^2 + ... \end{aligned} \qquad [3]$$

When the organ is nearly straight and vertical, there is no gravitropic response. So $A = 0$, $C = 0$ is a stable solution of the equation. Furthermore, as the behavior of the organ is independent of rotation around the vertical axis, the transformation $A \to -A$, $C \to -C$ should leave the system unchanged. This implies that all even-order terms in [3] disappear, yielding

$$\begin{aligned}\frac{\partial C(s,t)}{\partial t} &= \beta_1 A + \beta_3 A^3 + ... + \gamma_1 C + \gamma_3 C^3 + ... \\ &\quad + \delta_2 A^2 C + \delta_3 A C^2 + ... \end{aligned} \qquad [4]$$

This is the most general equation describing gravitropism of an elongated aerial organ.

For simplicity, we will first assume that the β and γ coefficients do not depend on position s or time t, i.e. that the sensitivities to angle and curvature are both time-independent and homogeneous. These assumptions have experimental support. Time-independence of the straightening response is envisageable in that tropic responses are fast in terms of the entire developmental timecourse of the organ (S1). Spatial homogeneity of the sensing capacity throughout the growth zone is supported by observations of the even distribution of statocytes or the response to high magnetic fields (22).

1.2 Test of two response functions: sine law (the A model) and exponential law. We may now compare two phenomenological ϕ functions that have been proposed in the literature, the sine law and the exponential law, to the general equation [4].

The sine law was defined by Sachs in the 19th century (see (3) for a review). Here then equation [2] can be rewritten as

$$\frac{\partial C(s,t)}{\partial t} = \alpha \sin A(s,t) \qquad [5]$$

where α is a parameter. Expanding $sin(A)$ as a power series (valid for any A) yields

$$\sin A = A - \frac{A^3}{3!} + \frac{A^5}{5!} + O(A^7) \qquad [6]$$

Since there are no even-order terms, the equation satisfies the symmetry condition mentioned above and the sine law is thus a special instance of equation [4]. In this work, we have used the approximation $\sin A \approx A$, for equation [5] giving

$$\partial C(s,t)/\partial t = -\beta A(s,t) \qquad [7]$$

Equation [7] is a mathematical specification of the hypothesis that the rate of local change in local curvature C is controlled only by a graviceptive term depending on the local inclination angle A. We have thus called this model the graviceptive model, or the *A* model (see also equation [3] in the main text).

We may now consider the exponential law postulated in the complete model of the tropic reaction in (20). This law is described by the following function

$$\frac{\partial C(s,t)}{\partial t} = \alpha\, e^{\frac{A-\pi/2}{A_1}} = \alpha\, e^{\frac{A}{A_1}} e^{-\frac{\pi}{2A_1}} \qquad [8]$$

The effect of this function becomes very small when A is less than $\pi/2 - A_1$ and thus only affects the start of the reaction. The power series of e^{A/A_1} is given by

$$e^{A/A_1} = 1 + \frac{A}{A_1} + \frac{1}{2}\left(\frac{A}{A_1}\right)^2 + \frac{1}{3!}\left(\frac{A}{A_1}\right)^3 + \frac{1}{4!}\left(\frac{A}{A_1}\right)^4 + ... \qquad [9]$$

Here even terms appear so this function violates the symmetries of the system and is therefore not a suitable model. This illustrates the importance of considering the symmetry of the problem when modeling especially when the exponential function is used.

1.3 First-order equation. Near $A(s,t) = 0$ and $C(s,t) = 0$, equation [4] can be linearized. This first order expression is in fact a second order approximation since we have seen previously that all the even terms disappear and the first cross-product terms A^2C and C^2A are third-order. The generalized equation of gravitropism at the second order is thus given by

$$\frac{\partial C(s,t)}{\partial t} = -\beta A - \gamma C \qquad [10]$$

For an initially straight organ clamped at the base and tilted with an initial angle A_0 from the vertical, the boundary conditions are then given by

$$A(0,t) = A(s,0) = A_0 \qquad [11]$$
$$C(s,0) = 0 \qquad [12]$$

Equation [10] is a mathematical specification of the hypothesis that the rate of change in local curvature C is controlled by a graviceptive term depending on local inclination angle A and a proprioceptive term depending on the sensing of local curvature by each organ segment C (while respecting the symmetry of the problem, and using a second order approximation). This new model has been therefore called the graviproprioceptive model, or the *AC* model (see also equation [5] in the main text).

1.4 Steady state and the dimensionless number B_l. The steady state of the equation [10] is given by

$$\frac{\partial C(s,t)}{\partial t} = 0 \qquad [13]$$
$$-\beta A(s,t) - \gamma C(s,t) = 0 \qquad [14]$$
$$C(s,t) = \partial_s A(s,t) \qquad [15]$$

As $A(s,t) = 0$ is forbidden by the boundary condition if $A_0 \neq 0$, there is only one steady solution

$$-\beta A(s,t) - \gamma \frac{\partial A(s,t)}{\partial t} = 0 \qquad [16]$$
$$A(s,t) = A_0 e^{-\frac{\beta s}{\gamma}} \qquad [17]$$

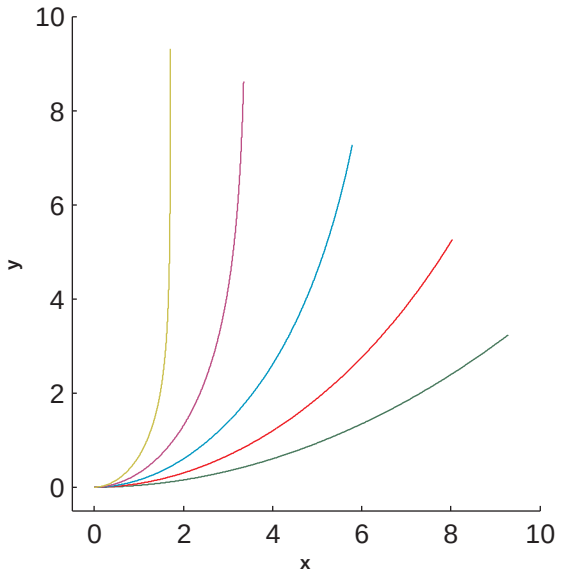

Fig. 1. Final shape of the *AC* model for different values of B_l with $L_{gz} = 10$. From the lower line (green) to the upper one (yellow) the values of B_l are respectively 0.5, 1, 2, 4 and 8.

Equation [17] thus defines the steady-state shape of the organ. Along the organ at steady state, the angle $A(s)$ decreases from A_0 to A_0/e ($\sim 0.37A_0$) over a length L_c given by

$$L_C = \frac{\gamma}{\beta} \qquad [18]$$

L_c is called the convergence length. It is then possible to designate a dimensionless number B_l by expressing L_c relatively to a characteristic effective length for bending L_{gz} (the length of the growth zone where active curving can be achieved):

$$B_l = \frac{\beta L_{gz}}{\gamma} \qquad [19]$$

Each value of B_l corresponds to one and only one specific shape (Figure 1). When B_l is a small number the apex of the organ cannot reach the vertical despite the fact that the graviceptive setpoint angle is $A = 0$, because the convergence length is too large compared to the length of the organ.

1.5 Timing of the movement and dimensionless number B_t. It is insightful to compare the time for the apex to reach the vertical to the time for the organ to converge to its final shape. Indeed when the organ reaches the vertical some time before convergence occurs, the organ may exhibit transient spatial oscillations.

A straightforward (under)estimation of the time for the apex to reach the vertical can be obtained by ignoring the proprioceptive process and further assuming that the angle A stays at its maximal value of A_0.

$$\frac{\partial C(s,t)}{\partial t} \approx -\beta A_0 \qquad [20]$$

with the solution

$$A(s,t) = A_0 - \int_{L_{gz}}^{s} ds \beta A_0 t \qquad [21]$$

i.e.,

$$A(0,t) = A_0 - \int_{L_{gz}}^{0} ds \beta A_0 t = A_0(1 - \beta L_{gz} t) \qquad [22]$$

Thus the time T_v to bring the apex to the vertical orientation ($A = 0$) is

$$T_v = \frac{1}{\beta L_{gz}} \qquad [23]$$

Likewise, when the gravi-proprioceptive term dominates, the convergence time T_c to the final shape is given by the characteristic time required by the organ to reach the steady state

$$T_c = \frac{1}{\gamma} \qquad [24]$$

It is now possible to define a dimensionless number for the movement as the ratio of the convergence time T_c and the vertical time T_v

$$B_t = \frac{\beta L_{gz}}{\gamma} \qquad [25]$$

By comparing equation [19] and equation [25] we see

$$B_l = B_t = B \qquad [26]$$

This "bending number" will quantify the number of transient overshoots that occur when the organ approaches the steady state as discussed in the main text.

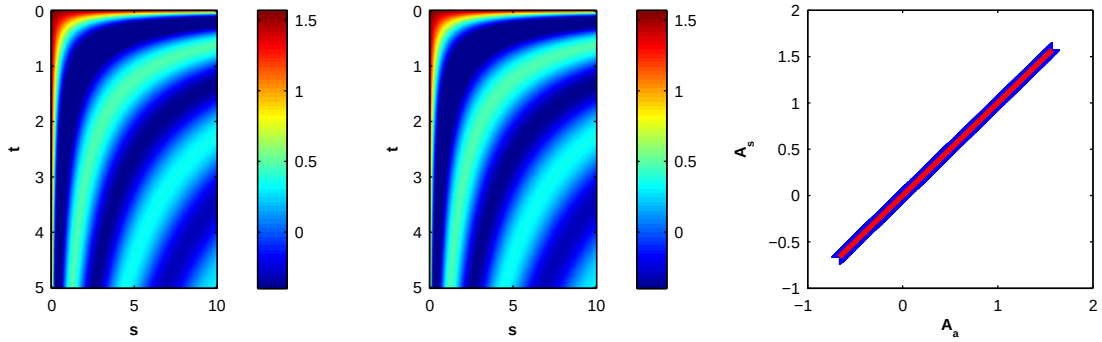

Fig. 2. Quantitative comparison between the analytical solution $A_a(s,t)$ (left panel) for the angle and the numerical solution $A_s(s,t)$ (middle panel) for the *A* model with $\beta = 1$ and $L_{gz} = 10$. Quantitative validation plot $A_a(s,t)$ vs $A_s(s,t)$ (right panel) with orthogonal linear fit (slope 1.0, intercept 0.0, R2 = 1.0).

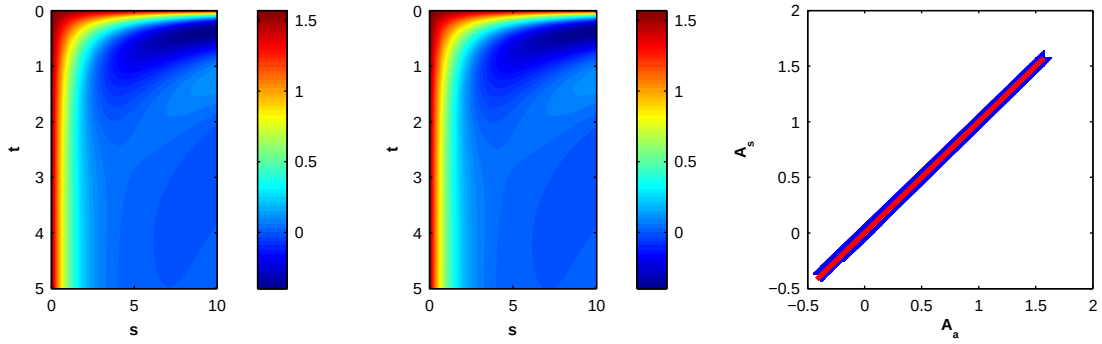

Fig. 3. Quantitative comparison between the analytical solution $A_a(s,t)$ (left panel) of the angle and the numerical solution $A_s(s,t)$ (middle panel) for the *AC* model with $B = 10$ and $L_{gz} = 10$. The quantitative validation plot $A_a(s,t)$ vs $A_s(s,t)$ (right panel) with orthogonal linear fit (slope 1.0, intercept 0.0, R2 = 1.0)

1.6 Analytical Solution and Numerical Simulations. The *A* model corresponds to the case, where the proprioceptive term is removed, and only the angle perception is kept:

$$\frac{\partial C(s,t)}{\partial t} = -\beta A \qquad [27]$$

With the initial condition $A(s, t = 0) = A_0$ this has the solution

$$A(s,t) = A_0\sqrt{\frac{\beta t}{s}}J_0\left(2\sqrt{\beta t s}\right) \qquad [28]$$

as can be seen by directly inserting it into the equation and performing the differentiations (S2) using

$$C(s,t) = \frac{\partial A(s,t)}{\partial s} \qquad [29]$$

This analytical solution A(s, t) of the *A* model [28] was compared to the angle space maps obtained through numerical simulations of Equation [27], for many sets of values for the two parameters. A typical example is shown in Figure S3. Again, no discrepancies were found between the analytical solution and the numerical experiments, so Equation 28 is correct and can be used to investigate the behavior of the *A* model and assess it against experimental data.

The analytical solution of the gravi-proprioceptive equation [10] with boundary conditions [11] and [12] are

$$A(s,t) = A_0 e^{-\gamma t}\sum_{n=0}^{\infty}\gamma^{n/2}\left(\frac{\beta s}{\gamma t}\right)^{-n/2}J_n\left(2\sqrt{\beta t s}\right) \qquad [30]$$

which can also be verified by direct differentiation, although more cumbersome (S2). This analytical solution A(s, t) of the *AC* model [30] was compared to the angle space map obtained through numerical simulations of Equation [10] for many sets of values for the two parameters. A typical example is shown in Figure S2. No discrepancies were found between the analytical solution and the numerical experiments, so Equation [30] is correct and can be used to investigate the behavior of the *AC* model and assess it against experimental data. The detailed mathematical derivation of the analytical solutions is available on ArXiv (S2).

2- Experiments

2.1 - Plant Materials and tilting experiments. Experiments were conducted in growth cabinets for etiolated wheat coleoptiles (*Triticum aestivum* cv. Recital) or controlled temperature greenhouses for the nine other types of plant organs - bean hypocotyl (*Phaseolus vulgaris*), sunflower hypocotyl (*Helianthus annuus*), pea epicotyl (*Pisum sativum*), tomato stem (*Solanum lycopersicum*), chili stem (*Capsicum annuum*), raspberry cane (*Rubus ideaus*), carnation inflorescence (*Dianthus caryophyllus*), and *Arabidopsis thaliana* inflorescences from a wild type (ecotype Col0) and its *pin1* mutant (a mutant of the PIN1 auxin efflux carier displaying reduced auxin longitudinal transport (11)). Plants were grown until a given developmental stage of the organ of interest (e.g until the beginning of inflorescence flowering for Arabidopsis in Figure 4). They were then tilted and clamped horizontally $A(s = 0, t) = \pi/2$ for all t under constant environmental conditions in the dark (to avoid interactions with phototropism). Number of replicates were 30 for wheat, 15 for *Arabidopsis* and 5 for all the other species. Published data were also reprocessed from similar experiments on *Impatiens glandilufera* stems by Pfeffer (35) and on poplar trunks (*Populus deltoides x nigra* cv I4551) by Coutand et al. (9).

2.2 - Detailed kinematics experiments. Time lapse photography was performed using a flash light, where the light was filtered to retain only green light, which did not stimulate any phototropic response. After initial tilting of the organ, the tropic movement was followed until a clear steady-state shape was achieved. One typical experiment on *Arabidopsis thaliana* is presented in Figure S5.A.

2.3 - Kinematics of Curving-Decurving. The central line of the organ was extracted from the pictures at successive times t and curvature C and curvilinear abscissa s at successive points along the central line were computed using a method described in refs (3,9). Space-time plots with color coding indicating the magnitude of the angle or the curvature were then generated to illustrate the pattern of the gravitropic movement.

2.4 Plant Material: phylogenetics of species studied. Eleven species were chosen from a broad taxonomical range of land angiosperms including monocots and dicots, see Figure S4. Different types of organs were studied: coleoptile, hypoctyl, epicotyl, inflorescence stems, or stems of vegetative shoots. The plants studied represent many of the growth habits of angiosperms, e.g. herbaceous plants, biennial shrubs and trees.

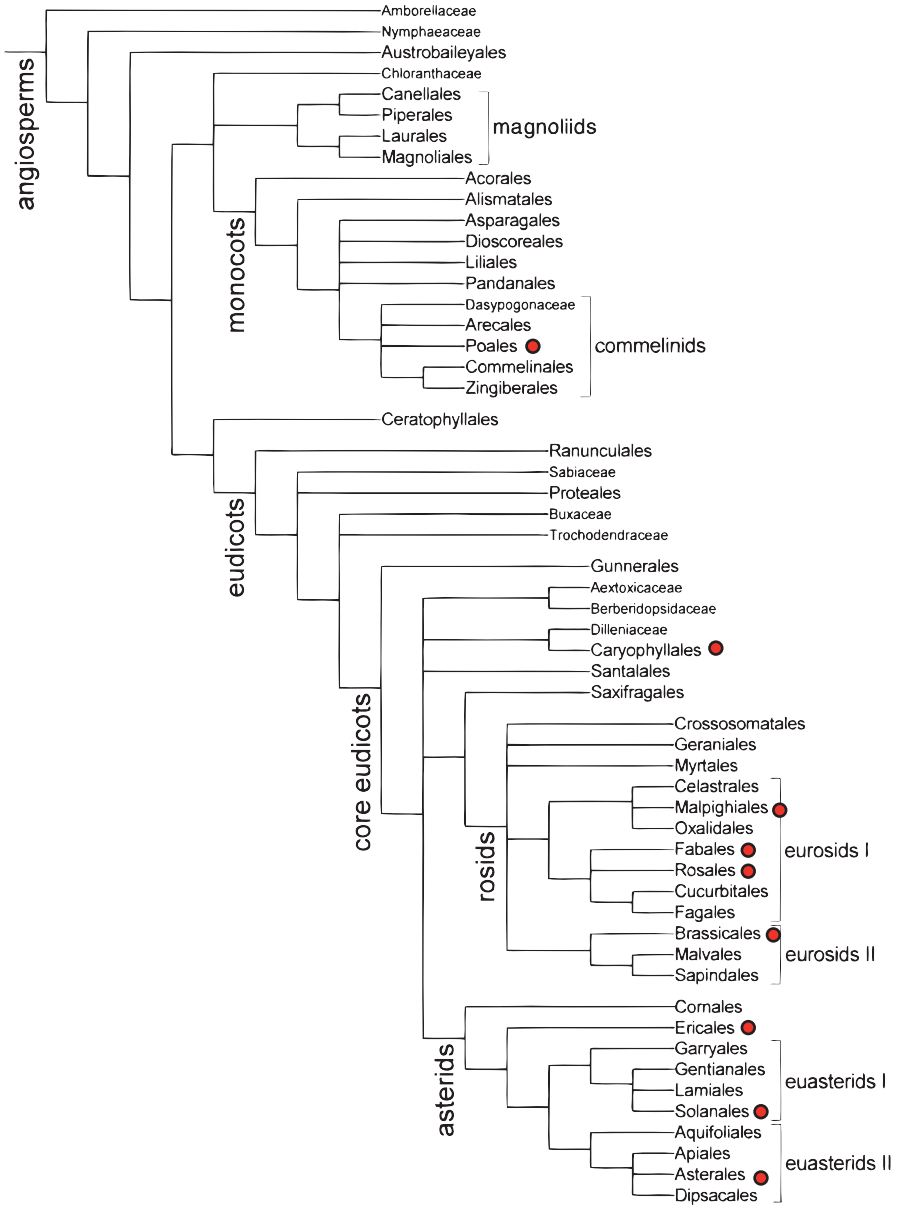

Fig. 4. Phylogenetic distribution of the species under study (modified from The Angiosperm Phylogeny (S3)). Families of the studied species are marked by a red dot.

2.5 Morphometric experiment and Characterization of transient oscillatory modes. Estimates of the bending number (through $B_l = L_{gz}/L_c$) and of the (transient) global mode M (Figure S5.B) were obtained. To estimate the length L_{gz} (the length of the organ along which active curving can take place), the first image of the kinematics just after tilting the organ was compared to the last one when the organ has reached a steady state (Figure 4). The distance between the apex and the most basal point with non-zero curvature on the last image gives the total length that was able to curve at the start of the experiment.This gives an approximation of the length of the growth zone L_{gz}.To get the convergence length L_c on the image of the steady state shape, the local orientation angle is taken from the point where the organ started to curve (Figure 4). Then the plot of $A(s)$ is fitted with an exponential function, $A_0 e^{-s/L_c}$. This fit gives a direct estimate of the convergence length to the vertical L_c. The measurement of the modes are illustrated in Figure S5.B. At a given time t the current mode is defined as the number of places below the apex where the tangent to the central line of the organ is vertical (Figure S5.B). In the example (Figure S5.A) the inflorescence of Arabidopsis displayed transient J then C shape and finally, just before convergence, an S shape. (Figure S5.B). Transient oscillatory modes were characterized by the mode number M defined as the maximal number of places in which the tangent to the central line of the organ is vertical simultaneously during the straightening mouvement. This transient state is the most curved state. In our experiments, only modes 0, 1 and 2 were observed. The value of mode M for (Figure S5.A) tilting experiment is thus M= 2.

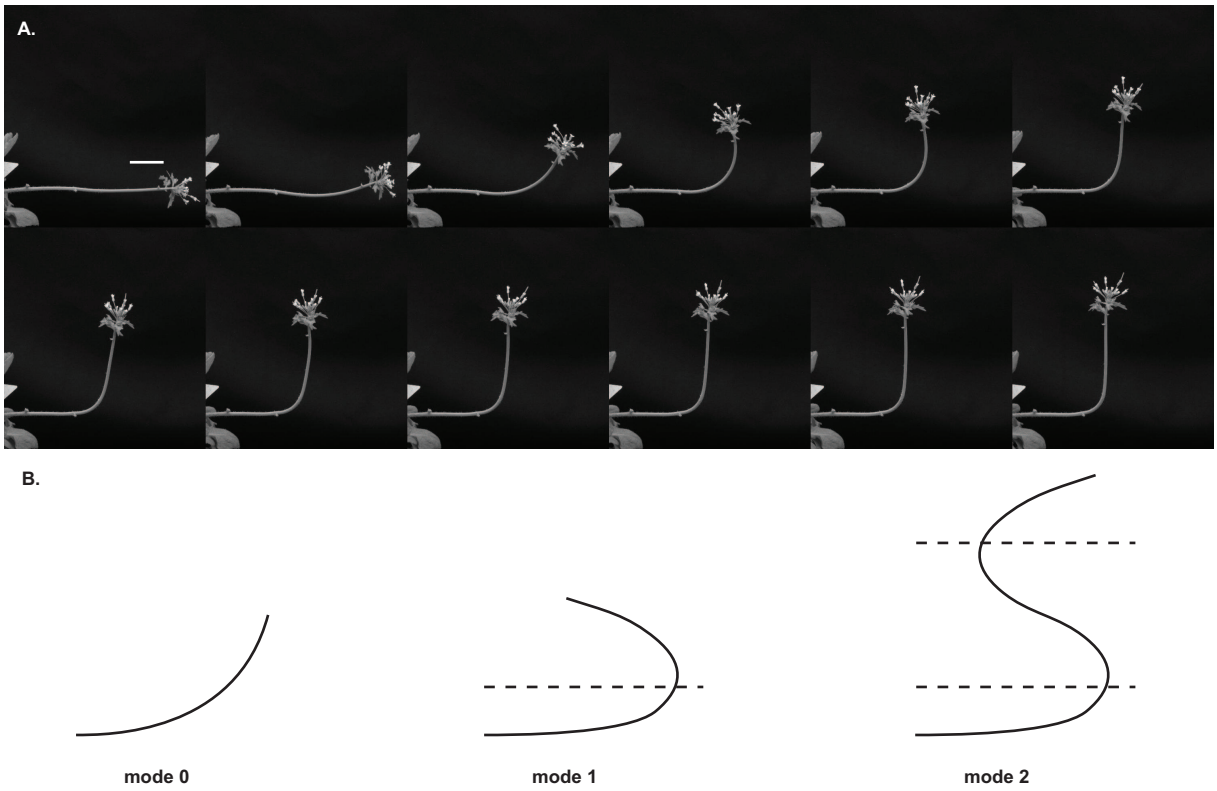

Fig. 5. A.Timelapse photographs of a tilting experiment on the inflorescence of *Arabidopsis thaliana* taken at 2- hour intervals. The apical part overshoots the vertical once 8 hours after tilting (4th image, C-shape). The white bar is 1 cm long. B.Quantification of the transient modes of the gravitropic movement. Mode M is the maximal number of places in which the tangent to central line of the organ crosses the vertical simultaneously. The curved line represents the gravitropic organ and the dashed lines represent different modes. No dashed line, mode 0 or J-shape; one dashed line, mode 1 or C shape; 2 dashed lines, mode 2 or S shape.

2.6 Quantitative Assessment and Statistical Fit.. The analytical expression for the angle A_{ac} of the *AC* model [10] was fitted to the experimental angle-space mapping numerically through a non linear optimization algorithm combining steepest gradient with random sampling of the parameter space (to avoid local minima), using the bending number estimated from the morphometric method as a starting value. The comparison between the measured angle dynamics $A_{exp}(s,t)$ and that predicted by the *AC* model $A_{ac}(s,t)$ was based on orthogonal functional linear regression, since the model prediction can also display random errors through the estimation of B (S4).

3. Detailed kinematics experiments and quantitative assessment of the AC model.

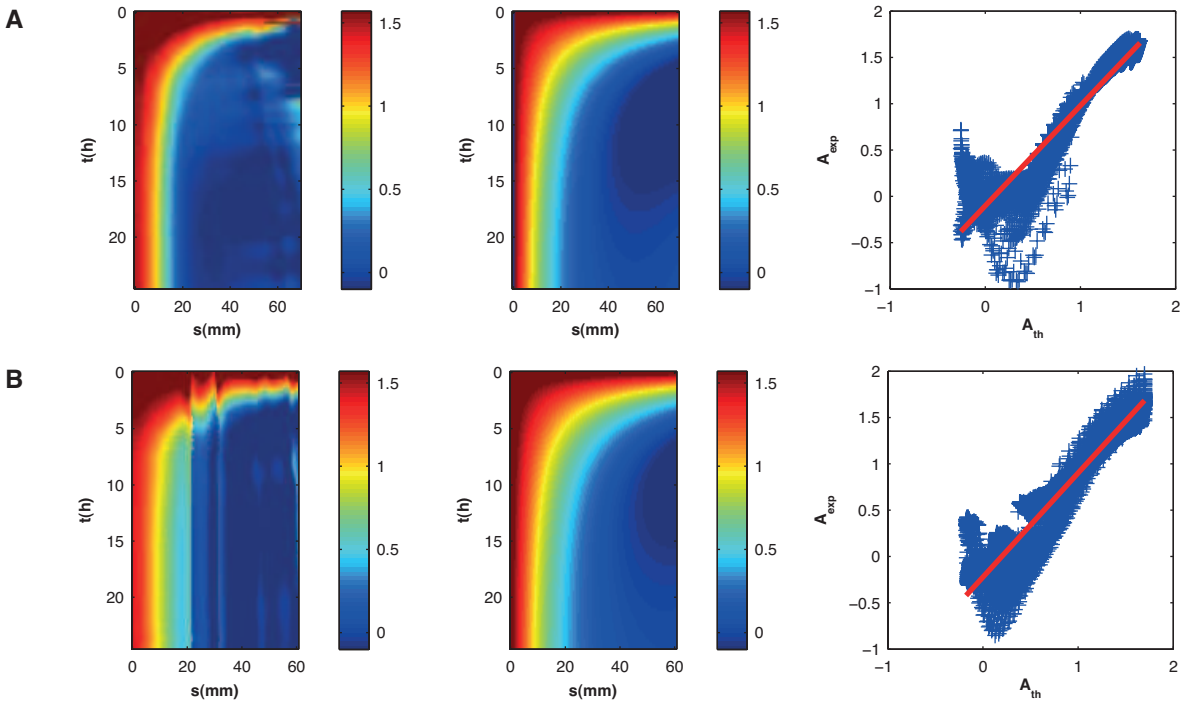

Fig. 6. Quantitative comparison between experimental (exp) and predicted angle spacetime map of A(s, t) in *Arabidopsis thaliana* inflorescence for the entire gravitropic response of two different individuals A and B. Experimental angle space-time map of $A_{exp}(s,t)$ (left panels), the angle space-time map predicted by the AC model $A_{th}(s,t)$ (middle panels) and quantitative validation plot of $A_{exp}(s,t)$ vs $A_{th}(s,t)$ (right panels). A. Orthogonal linear fit slope 1.14, intercept -0.067, R2 = 0.90. B. Orthogonal linear fit slope 1.17, intercept 0.017, R2 = 0.95.

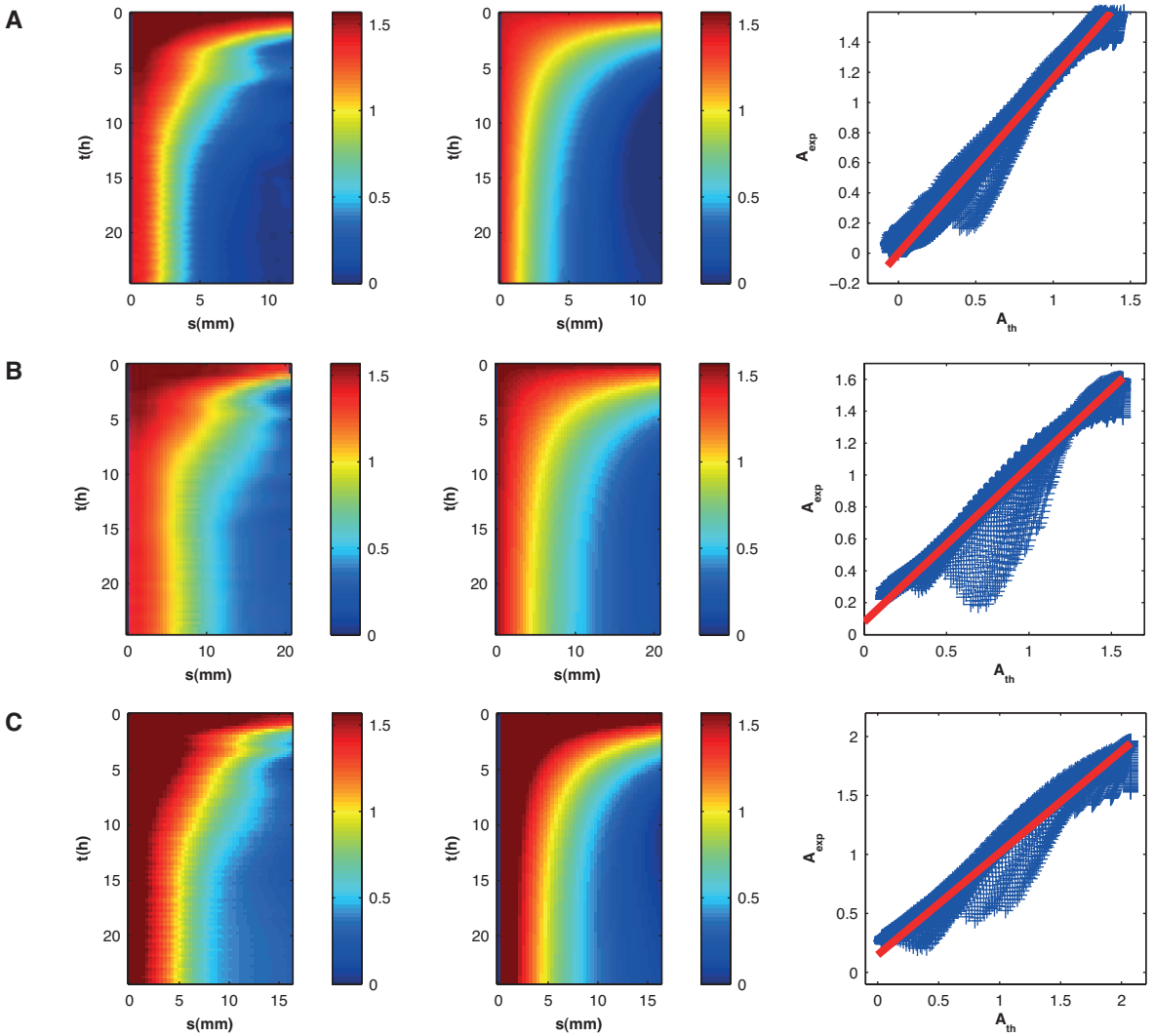

Fig. 7. Quantitative comparison between experimental (exp)and predicted (th) angle spacetime map of A(s, t) in wheat coleoptile for the entire gravitropic reponse of three different individuals A, B and C. Experimental angle spacetime map of $A_{exp}(s,t)$ (right panels), angle spacetime map predicted by the AC model $A_{th}(s,t)$ (middle panels) and quantitative validation plot $A_{exp}(s,t)$ vs $A_{th}(s,t)$ (right panels). A. Orthogonal linear fit slope 1.16, intercept 0.0003, R2 = 0.97. B. Orthogonal linear fit slope 0.97, intercept 0.078, R2 = 0.96. C. Orthogonal linear fit slope 0.88, intercept 0.15, R2 = 0.96.

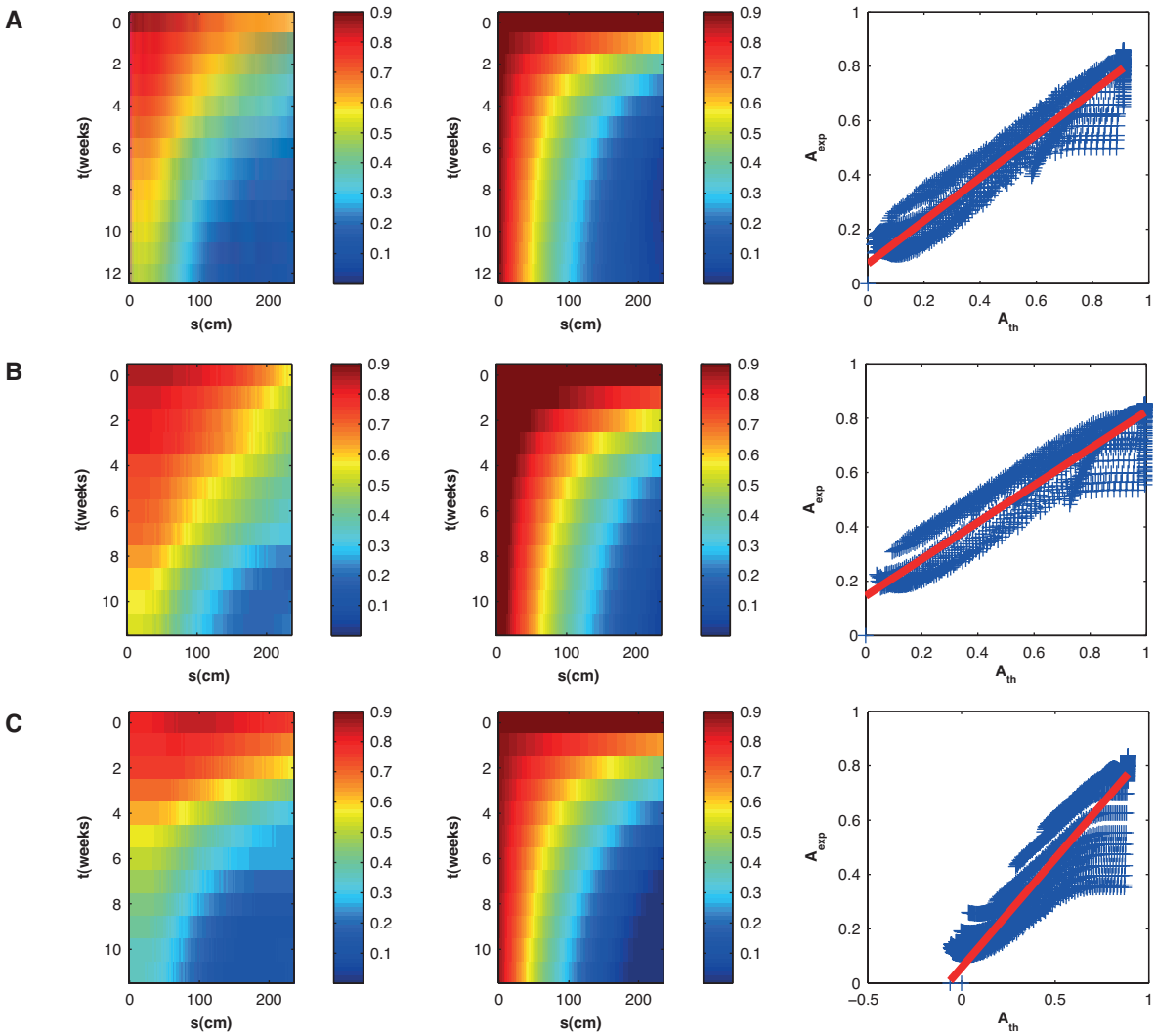

Fig. 8. Quantitative comparison between experimental (exp)and predicted (th) angle spacetime map of A(s, t) in poplar trunk for the whole straightening dynamics of three individuals A, B and C. Experimental angle spacetime map of $A_{exp}(s,t)$ (left panels), angle spacetime map predicted by the ACmodel $A_{th}(s,t)$ (middle panels) and quantitative validation plot $A_{exp}(s,t)$ vs $A_{th}(s,t)$ (right panels). A. Orthogonal linear fit slope 0.90, Intercept 0.037, R2=0.91, B. Orthogonal linear fit slope 0.88, Intercept 0.10, R2=0.86 and C. Orthogonal linear fit slope 0.80, Intercept 0.058, R2=0.80.

1. **Silk WK, Erickson RO (1978) Kinematics of hypocotyl curvature. *Am J Bot* 65(3):310-319.**

2. **Bastien R, Moulia B, Douady S, Bohr T (2012) Analytical Solution of the Proprio-Graviceptive equation for shoot gravitropism of plants arXiv:1210.3480 [q-bio.TO]**

3. **The Angiosperm Phylogeny Group (2003) An update of the angiosperm phylogeny group classification for the orders and families of flowering plants: Apg ii. *Botanical Journal of the Linnean Society* 141(4):399-436.**

4. **Dagnelie, P (2006) *Statistique théorique et appliquée. Tome 2. Inférence statistique à une et à deux dimensions* (2nd ed). De Boeck et Larcier, Brussels, Belgium. French**

Supporting Information

Bastien et al. 10.1073/pnas.1214301109

Movie S1. Gravitropic movement of a wheat coleoptile, after an initial tilting at 90° from the vertical. Note that this wheat coleoptile never overshot the vertical during the straightening process. Other coleoptiles in the experiment did not even reach the vertical even at their tip (not shown in the movie).

Movie S1

Movie S2. Gravitropic movement of an inflorescence of *A. thaliana* after an initial tilting at 90° from the vertical. The inflorescence of *A. thaliana* exhibited a transient C shape during the straightening process and overshot the vertical.

Movie S2

Movie S3. Solution of the *A* model. The color (from blue to red) codes for the absolute value of the curvature C(s,t). The simulated organ never reaches a steady state and oscillation increases along the organ.

Movie S3

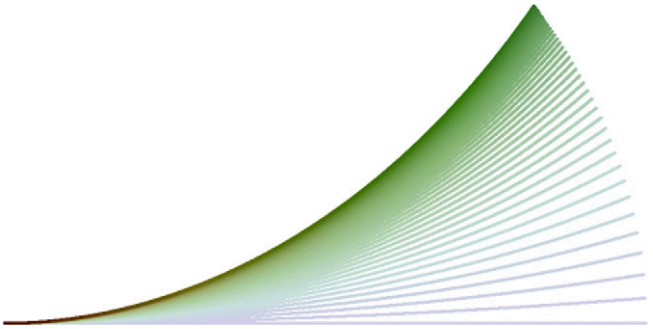

Movie S4. Solution of the *AC* model, $B = 1$. The color (from blue to red) codes for the absolute value of the curvature C(s,t). The simulated organ reaches a steady state but does not reach the vertical.

Movie S4

Movie S5. Solution of the *AC* Model, $B = 10$. The color (from blue to red) codes for the absolute value of the curvature C(s,t). The simulated organ reaches a steady state after exhibiting a transient S-shaped mode during the process.

Movie S5

Other Supporting Information Files

SI Appendix (PDF)